A hybrid hydrochromic molecular crystal applicable to invisible ink with high reversibility

Yao Huang, Tie Zhang, Lu-Lu Chu, Yi Zhang*, Jia-Zhen Ge*, Da-Wei Fu*.

(Ordered Matter Science Research Center, Jiangsu Key Laboratory for Science and Applications of Molecular Ferroelectrics, Southeast University, Nanjing, 211189, P.R. China)

Experimental section

Synthesis of $(C_8H_{20}N_2)[Mn(NCS)_4(H_2O)_2]$.

All the commercially obtained experimental reagents are of analytical grade and were used without further purification. To obtain (TMPZ)Br (TMPZ =1,1,4,4-Tetramethylpiperazinium), dimethylamine was dissolved in 100 ml acetonitrile and bromochloroethane (0.10 mol) was added dropwise. The resulting mixture was stirred for 24 hours in an oil bath, then the solvent was removed under pressure reduction to obtain the colorless solid product (TMPZ)Br. Bromine and carbonate ions were removed by adding an appropriate amount of silver carbonate and hydrochloric acid. To synthesize $(C_8H_{20}N_2)[Mn(NCS)_4(H_2O)_2]$, $MnCl_2$ (1.2584 g, 10.0 mmol) and KSCN (2.915 g,30 mmol) was added to the solution of (TMPZ) (1.44 g, 10.0 mmol) and 40% HCl (1.0 mL) under stirring. The crystal was synthesized by the solvent evaporation method, and the colorless transparent crystal was obtained after two weeks at room temperature.

Single crystal X-ray crystallography (XRD).

The single-crystal XRD data of compound $(C_8H_{20}N_2)[Mn(NCS)_4(H_2O)_2]$ from 198 K to 393 K were obtained by a Rigaku Varimax TM DW diffractometer with Mo Ka radiation (λ = 0.71073 Å) using the ω scan technique. The crystallographic data were processed through direct methods and refined by full-matrix. Least-squares methods using the SHLXTL-97 procedure.

Thermal and Phase Stabilities.

The pressed-powder pellets with silver glue painted were used as electrodes to testing the dielectric constants within the frequency range of 0.5 kHz to 1 MHz, using a TongHui TH2828A impedance analyzer under an applied field of 1.0 V in the temperature range of 173-373 K. In the differential scanning calorimetry (DSC) experiments, the dry powder of $(C_8H_{20}N_2)[Mn(NCS)_4(H_2O)_2]$ was put in aluminum crucibles and then put into the PerkinElmer Diamond DSC instrument. The measurement was carried out under nitrogen at atmospheric pressure with a heating and cooling rate of 20 $K \bullet min^{-1}$. Thermogravimetric analyses (TGA) of the obtained polycrystalline powder were performed on a METTLER TOLEDO STARe System to test the stability in the temperature range of 298-773 K with a heating rate of 20 $K \bullet min^{-1}$. The Powder X-ray diffraction (PXRD) patterns were recorded on Rigaku Ultima IV multipurpose X-ray diffraction system, they were also compared with the profiles

obtained from the single-crystal structure at room temperature, which were generated by Mercury version 3.5.1. which matches well with the simulated patterning.

Infrared (IR) and Ultraviolet (UV) spectroscopy.

The Fourier-transform infrared (FT-IR) spectra of the samples were characterized by a Nicolet 4700 FTIR Spectrometer. The specimens were prepared by mixing the powdered samples with dried KBr powder, followed by the application of a force of approximately 40 MPa to form pellets. The spectra were collected over a spectral range of 3600–400 cm^{-1}. Color changes of synthesized **1** at high temperature were investigated by adding the powder into sample tray, followed by heating to different temperatures from 298 to 393 K in 20 K steps in a digital muffle furnace, and maintaining each temperature for 5 min. After keeping the powdered samples at different temperatures for different periods, the sample tray was removed and allowed to cool to room temperature, the color change of the powder sample was recorded by camera.

Results and discussion

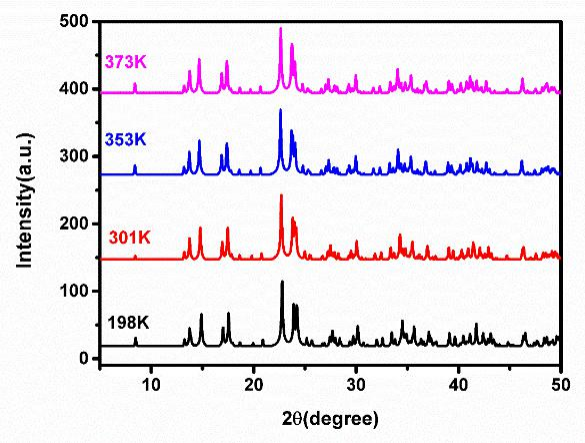

Figure S1. The simulated PXRD spectra of sample at varing temperatures. the simulated plots match well with the measured ones at all temperatures.

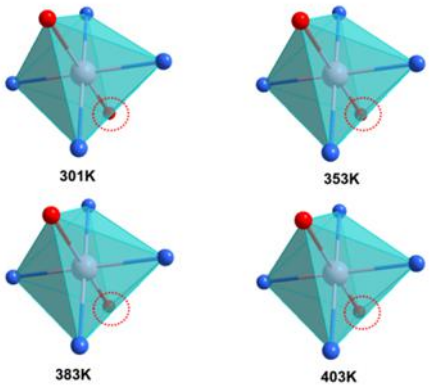

Figure S2. Slight changes in the shape of the octahedral structure at various temperatures observed in the c-axis.

The deuterium experiments verified to some extent that the discoloration of the organic-inorganic hybrid structure was caused by the reversible gain and loss of coordinated water. Besides, compound 1 is heated to 373 K and then quickly cooled to room temperature. The UV absorption spectra (Fig. S2a) at these two temperatures are the same, so heating is not the necessary input for the discoloration and merely serves to accelerate dehydration. UV absorption spectra after a heating-cooling cycle.

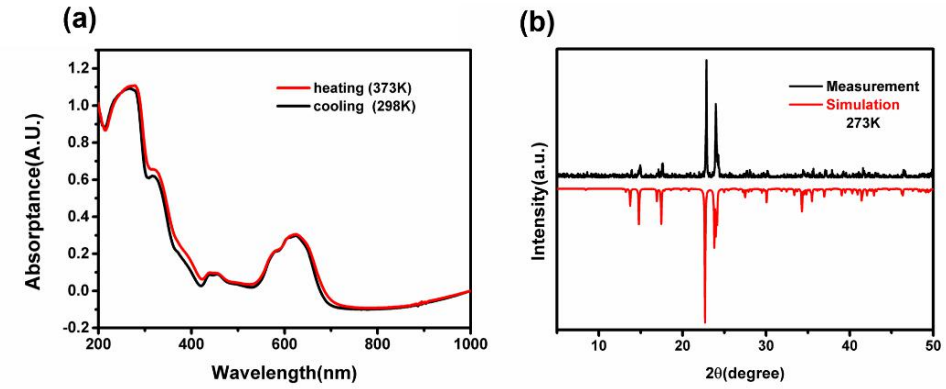

Figure S3. (a). Comparison between measurement and simulation PXRD of $(C_8H_{20}N_2)[Mn(NCS)_4(H_2O)_2]$ at 273 K(b), which shows good match and purity.

XPS

Due to the different chemical environments of Mn, the electron the binding energy of the inner shell changes, or may be caused by the combination of different types or quantities of elements with atoms. According to the atomic sensitivity factor method, the relative atomic concentrations of Mn and O before and after discoloration can be calculated that the concentration of coordinated oxygen in the blue sample is reduced, which proves that part of coordinated water is lost in the discoloration process.

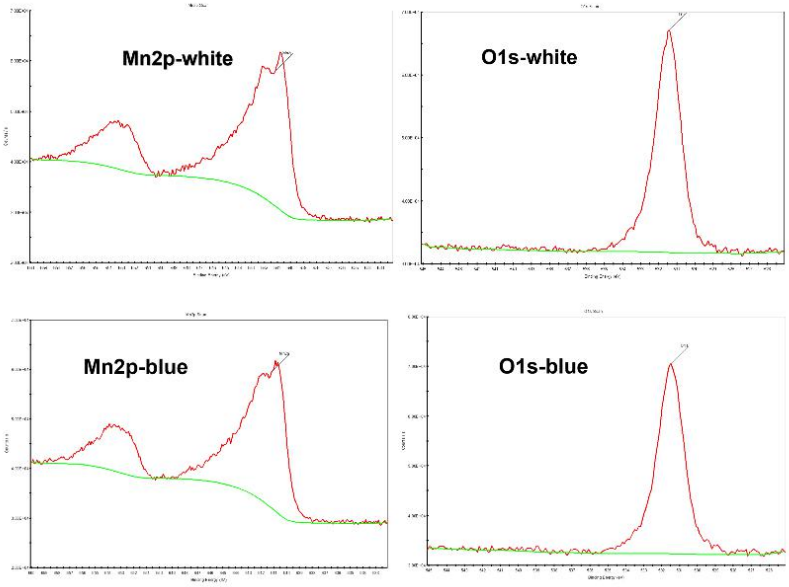

Figure S4. The XPS intensity of the O&Mn before and after dehydration.

The peak intensity is proportional to the number of electrons in the energy level, the photoionization interface of electrons in the energy level, and the concentration of these atoms in the sample. The fitting peak area is used to deal with it.

$$Cx = \frac{Ix}{Sx} : \frac{\sum Ii}{\sum Si}$$

$$n1 : n2 = \frac{I1}{S1} : \frac{I2}{S2}$$

Dielectric and DSC

When the temperature rises to 301 K and 393 K, compound **1** still crystallized in the monoclinic space group $P2_1/c$. The crystal has similar cell parameters at the three temperatures (Table S2-7), by comparing the bond length and angle at different temperatures, the thermal vibration of atoms becomes a more intense disorder. The position of the O atom in the unit cell and the angle of O and the N-N plane changes obviously. The octahedral deformation of $[Mn(NCS)_4(H_2O)_2]^{2-}$ configuration occurs in an ordered/disordered phase transition, accompanied by molecular dynamics, this DSC mode and dielectric curves perfectly illustrate the reversible conversion, which is a powerful factor in finding excellent bistable switches.

TG analysis of 1

For exploring the loss of coordinated water content (part or all), the sample was analyzed by thermogravimetric analysis and in-situ variable temperature infrared spectroscopy. Fig. S5c shows compound **1** experienced two-weight losses below 773 K. 4.9% of the weight at 328-348 K reflects the loss of water. The temperature range is consistent with the temperature range in which the sample begins to change color when heated. The single molecular structure contains about 7.7% coordinated water, so the coordinated water in the crystal is partially lost above 333 K. When the temperature rises to 443 K, $(TMPZ)^{2+}$ begins to be removed, leading to the gradual collapse of the skeleton. From the PXRD results of the blue sample, the structure of compound 1 in this state has changed obviously, which is also consistent with the results of the first TG weightlessness. The discoloration phenomenon is a reversible de-coordinated and re-coordinated process of water.

The IR spectrum studies of white and blue samples were performed in the 4000-500 cm^{-1} frequency regions as shown in Fig. S5d, respectively. With the loss of coordinated water (blue), the absorption intensity at 3600 cm^{-1} decreases significantly, effectively proved the partial loss of coordinated water distribution before and after dehydration.

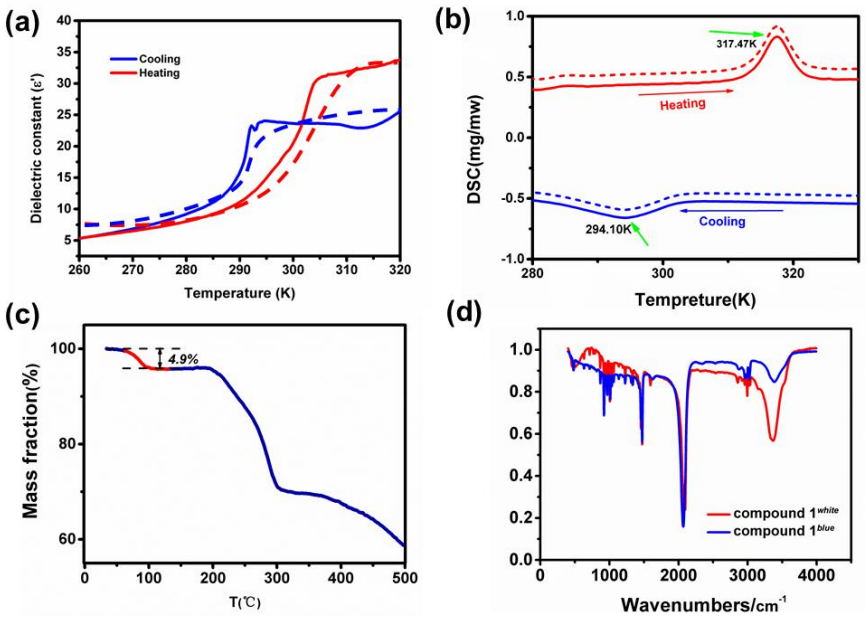

Figure S5. (a) The dielectric measurement (1 MHz) and DSC (b) curves of powder tablet of ($C_8H_{20}N_2$) $[Mn(NCS)_4(H_2O)_2]$ under heating and cooling in two reversible cycles; (c)TG curves of compound **1** showing two steps of weight loss. It is completely repeated below the temperature of 400K by being exposed to the air for 2 minutes, and the reversible structure transition reflected by TG is consistent with PXRD; The IR spectrum of compound **1**, (d).

The Hirshfeld surfaces mapped over d_{norm} and the corresponding two-dimensional fingerprint plots for compound **1** at 198 K and 393 K were performed using the CrystalExplorer program. Hydrogen bond contact is mainly concentrated on the coordination of water molecules on both sides. The proportion of hydrogen bond can be seen by comparing the deep red depression in Figure S6(c) and (d) has changed obviously with the increasing temperature. When compound **1** is exposed to a higher temperature, the loss of coordinated water also leads to the weakening of the hydrogen bonding force.

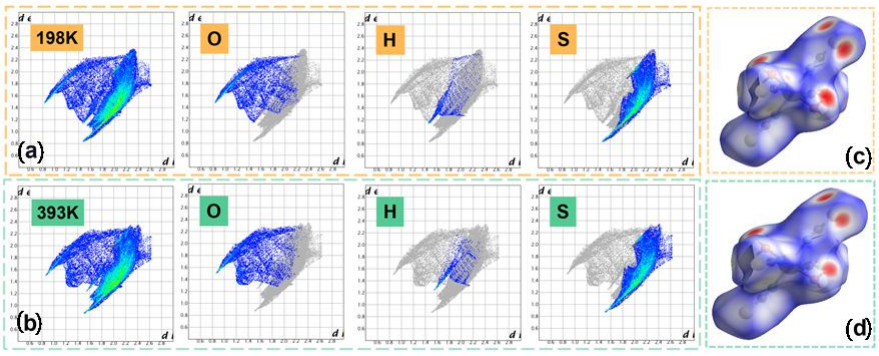

Figure S6. The Hirshfeld surfaces mapped over d_{norm} and the corresponding two-dimensional fingerprint plots for compound **1** at 198 K (a,c) and (b,d) 393 K.

Humidity comparative tests

In the process of observing compound **1** from blue to white, we carried out several comparative tests. At room temperature, the time of the sample from blue to white differ in different humidity, a series of dynamic analyses of this process was carried out. Expose the blue sample to different humidity (25%-85%), and change every five percentage points, record the time from blue to white to conclude: the greater the humidity, the shorter the time required for the color change, which indirectly reflects the correlation between the color change of the sample and the loss of water. While considering the influence of humidity, attention was also paid to exclude the influence of temperature on turning back.

To verify that discoloration is not caused by heating unilaterally, but because of the loss of coordinated water under certain forces with the influence of humidity change in the external environment, the pure powder was placed in a closed vacuum container at room temperature, and a small amount of phosphorus pentoxide was added at the bottom, which is easy to absorb moisture and the capacity of dehydration is very strong. One hour later, most of the powder turned blue, which was consistent with the mechanism of discoloration caused by heating. When it is in a certain humidity environment, the coordinated water and the external water reach a balance, so it will not be released to the outside as a supplement.

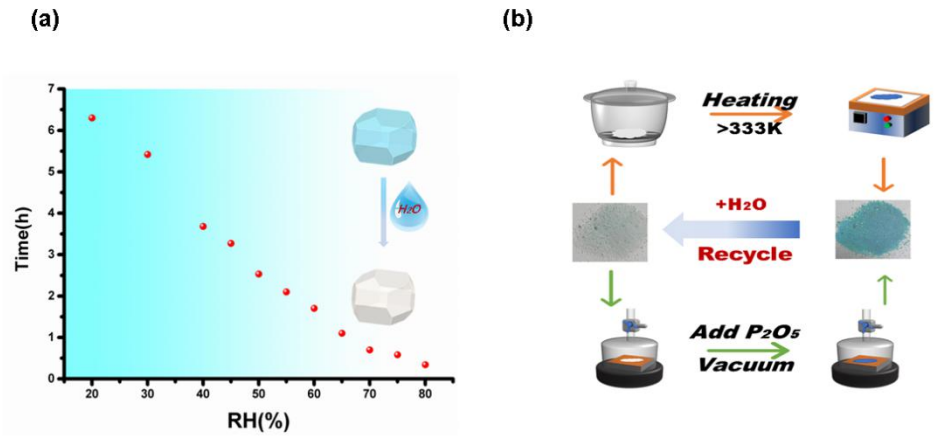

Figure S7. (a) The time of the same batch of powder from blue to colorless was tested under different environmental humidity, and the other experimental conditions such as temperature, powder content and discoloration degree are consistent; (b) Discoloration conditions of compound **1** in different environments.

Table S1. Crystal data and structure refinement for $(C_8H_{20}N_2)$ $[Mn(NCS)_4(H_2O)_2]$ **(1).**

Empirical formula	$C_{12}H_{24}MnN_6O_2S_4$	$C_{12}H_{24}MnN_6O_2S_4$	$C_{12}H_{24}MnN_6O_2S_4$
Formula weight	467.55	467.55	467.55
Temperature/K	198	301	393
Crystal system	monoclinic	monoclinic	monoclinic
Space group	$P2_1/c$	$P2_1/c$	$P2_1/c$
a/Å	11.1894(3)	11.2454(9)	11.3229(13)
b/Å	7.3513(1)	7.4131(4)	7.5060(4)
c/Å	13.8269(3)	13.8459(11)	13.8159(9)
α/°	90	90	90
β/°	111.428(3)	111.503(9)	111.721(8)
γ/°	90	90	90
Volume/Å^3	1058.74(5)	1073.91(13)	1090.84 (13)
Z	2	2	2
F(000)	486.0	486.0	486.0
Final R indexes	R_1 = 0.0357	R_1 = 0.0412	R_1 = 0.0695
[I>=2σ (I)]	wR_2 = 0.1004	wR_2 = 0.1603	wR_2 = 0.2839
GOF	1.032	0.935	1.002

Table S2. Bond Lengths for $(C_8H_{20}N_2)$ $[Mn(NCS)_4(H_2O)_2]$ (**1**) at 198 K.

Atom	Atom	Length/Å	Atom	Atom	Length/Å
Mn1	O8	2.2069(9)	N11	$C10^2$	1.5029(14)
Mn1	$O8^1$	2.2069(9)	N11	C9	1.5037(14)
Mn1	N7	2.2182(11)	N11	C13	1.5078(16)
Mn1	$N7^1$	2.2182(11)	N11	C12	1.5050(18)
Mn1	N4	2.1707(13)	N7	C6	1.1510(17)
Mn1	$N4^1$	2.1707(13)	N4	C3	1.160(2)
S2	C3	1.6272(15)	C10	C9	1.5141(18)
S5	C6	1.6418(12)			

Table S3. Bond Angles for $(C_8H_{20}N_2)$ $[Mn(NCS)_4(H_2O)_2]$ (**1**) at 198 K.

Atom	Atom	Atom	Angle/°	Atom	Atom	Atom	Angle/°
$O8^1$	Mn1	O8	180.0	$N4^1$	Mn1	N4	180.0
N7	Mn1	O8	91.72(4)	C9	N11	$C10^2$	107.91(10)
$N7^1$	Mn1	O8	88.28(4)	C13	N11	$C10^2$	112.12(9)
$N7^1$	Mn1	$O8^1$	91.72(4)	C13	N11	C9	111.93(9)
N7	Mn1	$O8^1$	88.28(4)	C12	N11	$C10^2$	108.20(9)
N7	Mn1	$N7^1$	180.0	C12	N11	C9	108.81(9)
N4	Mn1	$O8^1$	87.38(5)	C12	N11	C13	107.77(11)

N4	Mn1	O8	92.62(5)	C6	N7	$Mn1^{1}$	158.21(12)
$N4^{1}$	Mn1	$O8^{1}$	92.62(5)	C3	N4	Mn1	156.95(12)
$N4^{1}$	Mn1	O8	87.38(5)	C9	C10	$N11^{2}$	113.02(9)
$N4^{1}$	Mn1	N7	91.51(5)	C10	C9	N11	112.42(9)
$N4^{1}$	Mn1	$N7^{1}$	88.49(5)	N7	C6	S5	178.27(12)
N4	Mn1	N7	88.49(5)	N4	C3	S2	178.28(12)
N4	Mn1	$N7^{1}$	91.51(5)				

Table S4. Bond Lengths for ($C_8H_{20}N_2$) [$Mn(NCS)_4(H_2O)_2$] (**1**) at 301 K.

Atom	Atom	Length/Å	Atom	Atom	Length/Å
Mn1	O5	2.206(2)	N4	C6	1.503(3)
Mn1	$O5^{1}$	2.206(2)	N4	$C7^{2}$	1.505(3)
Mn1	$N1^{1}$	2.215(3)	N4	C7	1.502(3)
Mn1	N1	2.215(3)	N4	C8	1.500(3)
Mn1	$N2^{1}$	2.180(3)	C6	C7	1.510(4)
Mn1	N2	2.180(3)	C7	$N4^{2}$	1.505(3)
S2	C9	1.615(3)	N1	C6	1.146(4)
S3	C6	1.631(3)	C9	N2	1.149(4)

Table S5. Bond Angles for ($C_8H_{20}N_2$) [$Mn(NCS)_4(H_2O)_2$] (**1**) at 301K.

Atom	Atom	Atom	Angle/°	Atom	Atom	Atom	Angle/°
$O5^{1}$	Mn1	O5	180.00(14)	N2	Mn1	$N2^{1}$	180.0
$O5^{1}$	Mn1	N1	91.73(10)	C6	N4	$C7^{2}$	107.80(18)
O5	Mn1	N1	88.27(10)	CC	N4	C6	111.9(2)
O5	Mn1	$N1^{1}$	91.73(10)	CC	N4	$C7^{2}$	112.1(2)
$O5^{1}$	Mn1	$N1^{1}$	88.27(10)	C8	N4	C6	108.1(2)
$N1^{1}$	Mn1	N1	180.0	C8	N4	$C7^{2}$	108.4(2)
$N2^{1}$	Mn1	$O5^{1}$	92.14(11)	C8	N4	C7	108.4(2)
N2	Mn1	O5	92.14(11)	N4	C6	C7	112.9(2)
$N2^{1}$	Mn1	O5	87.86(11)	$N4^{2}$	C7	C6	112.1(2)
N2	Mn1	$O5^{1}$	87.86(11)	C6	N1	Mn1	157.9(3)
N2	Mn1	$N1^{1}$	88.43(11)	N2	C9	S2	178.1(3)
$N2^{1}$	Mn1	N1	88.44(11)	C9	N2	Mn1	157.5(3)
N2	Mn1	N1	91.57(11)	N1	C6	S3	178.5(3)
$N2^{1}$	Mn1	$N1^{1}$	91.56(11)				

Table S6. Bond Lengths for ($C_8H_{20}N_2$) [$Mn(NCS)_4(H_2O)_2$] (**1**) at 393 K.

Atom	Atom	Length/Å	Atom	Atom	Length/Å
Mn1	O13[1]	2.207(3)	N10	C9	1.496(4)
Mn1	O13	2.207(3)	N10	C8	1.503(4)
Mn1	N4	2.158(4)	N10	C12	1.494(4)
Mn1	N4[1]	2.158(4)	N10	C11	1.495(6)
Mn1	N7	2.209(4)	C3	N4	1.149(6)
Mn1	N7[1]	2.209(4)	C6	N7	1.132(4)
S2	C3	1.622(5)	C9	C8[2]	1.531(6)
S5	C6	1.633(4)	C8	C9[2]	1.531(6)

Table S7. Bond Angles for ($C_8H_{20}N_2$) [$Mn(NCS)_4(H_2O)_2$] (**1**) at 393 K.

Atom	Atom	Atom	Angle/°	Atom	Atom	Atom	Angle/°
O13	Mn1	O13[1]	180.00(15)	N7	Mn1	N7[1]	180.0
O13[1]	Mn1	N7[1]	89.20(14)	C9	N10	C8	107.2(3)
O13	Mn1	N7[1]	90.80(14)	C12	N10	C9	113.3(2)
O13[1]	Mn1	N7	90.80(14)	C12	N10	C8	112.1(3)
O13	Mn1	N7	89.20(14)	C12	N10	C11	108.5(3)
N4	Mn1	O13	91.12(16)	C11	N10	C9	108.1(3)
N4[1]	Mn1	O13	88.87(16)	C11	N10	C8	107.5(3)
N4[1]	Mn1	O13[1]	91.13(16)	N4	C3	S2	178.7(4)
N4	Mn1	O13[1]	88.88(16)	C3	N4	Mn1	159.4(4)
N4	Mn1	N4[1]	180.0	N7	C6	S5	177.6(4)
N4[1]	Mn1	N7	88.50(16)	N10	C9	C8[2]	111.9(3)
N4[1]	Mn1	N7[1]	91.50(16)	C6	N7	Mn1	157.7(4)
N4	Mn1	N7	91.50(16)	N10	C8	C9[2]	112.1(3)
N4	Mn1	N7[1]	88.50(16)				